THE JOURNAL OF PHYSICAL CHEMISTRY C

Article

pubs.acs.org/JPCC

Visible Photoluminescence Components of Solution-Grown ZnO Nanowires: Influence of the Surface Depletion Layer

Jiandong Fan,[†] Frank Güell,[†] Cristian Fábrega,[‡] Andrew Fairbrother,[‡] Teresa Andreu,[‡] Antonio M. López,[§] Joan Ramón Morante,[†,‡] and Andreu Cabot*[,†,‡]

[†]Departament Electronica, Universitat de Barcelona, Barcelona 08028, Spain

[‡]Catalonia Institute for Energy Research, IREC, Sant Adria del Besos, Barcelona 08930, Spain

[§]Departament d'Enginyeria Electrónica, Universitat Politècnica de Catalunya, EPSEVG, Avinguda Victor Balaguer s/n, 08800 Barcelona, Spain

Supporting Information

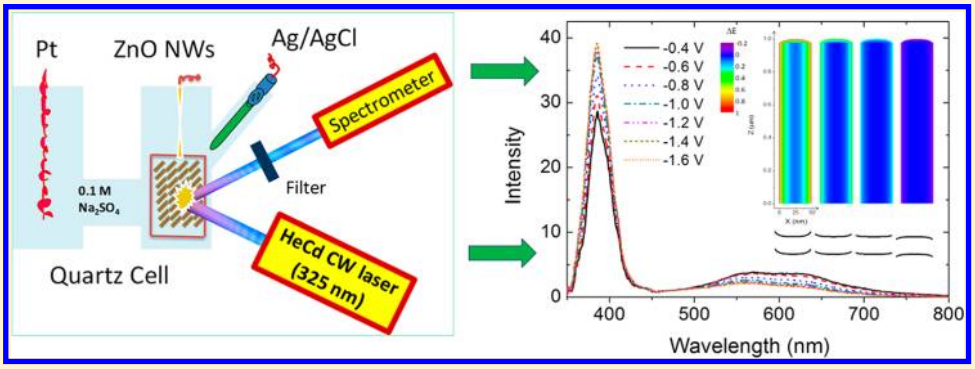

ABSTRACT: Arrays of electrodeposited ZnO nanowires (NWs) were used to illustrate the dependence of the ZnO visible photoluminescence (PL) emission on the extension of the surface depletion layer and obtain further insight into the localization of the related states. With this goal in mind, three sets of measurements were carried out: (i) analysis of the PL spectra of ZnO:Cl NWs as a function of their carrier concentration; (ii) analysis of the PL spectra of ZnO:Cl/ZnO core−shell NWs as a function of the thickness of their intrinsic ZnO shell; (iii) in situ analysis of the PL dependence on the polarization of ZnO:Cl photoelectrodes. The obtained experimental results evidenced that the yellow and orange emissions from electrodeposited ZnO NWs are correlated with the extension of the NWs surface depletion region. This result points out the surface localization of the states at the origin of these transitions. On the other hand, the green emission that dominates the visible part of the PL spectra in annealed ZnO NWs showed no dependence on the surface band bending, thus pointing toward its origin in the bulk.

1. INTRODUCTION

Zinc oxide, having a wide direct band gap (3.37 eV) and large exciton binding energy (60 meV), is an excellent candidate for optoelectronic applications, such as light-emitting diodes,[1] laser diodes[2] and solar cells.[3] Its wide range of applications has motivated a comprehensive characterization of its properties and an intensive investigation of its potential applications. Nevertheless, a lack of consensus on important optical properties, such as the origin of its visible photoluminescence (PL) emission, still exists.[4−6] The various contributions to the visible emission has been associated with oxygen vacancies,[7−14] oxygen antisites, oxygen interstitial,[15,16] zinc vacancy,[17−20] zinc interstitials,[21,22] trapped OH^- groups,[18] and even Cu impurities.[23] On the other hand, evidence exists that the intensity of some contributions to the visible emission band depends on the material surface-to-bulk ratio.[24−29] Such experimental evidence has been rationalized by considering the surface localization of the related states, their surface activation by the hole accumulation at the surface depletion region, or the promotion of slower recombination processes by charge separation in the built-in electric field surface layer.[9−12,30−36] The surface band bending has also been reported to activate indirect band-to-band transitions.[37]

The controversy about the association of the transitions behind the visible PL emission is in part originated from the strong dependence of the PL emission on the ZnO preparation techniques, the specific growth parameters used, and the applied postgrowth treatments.[38] The large variety of methods available for the synthesis of ZnO crystals with different geometries and sizes does not help to solve this puzzle. In this scenario, a particularly interesting geometry at the nanometer scale is that of nanowires (NWs).[4,39,40] Its interest originates from the potential concurrence of a high electrical conductivity and a high surface area in the same structure. ZnO NWs can be

Received: March 13, 2012
Revised: August 14, 2012
Published: August 15, 2012

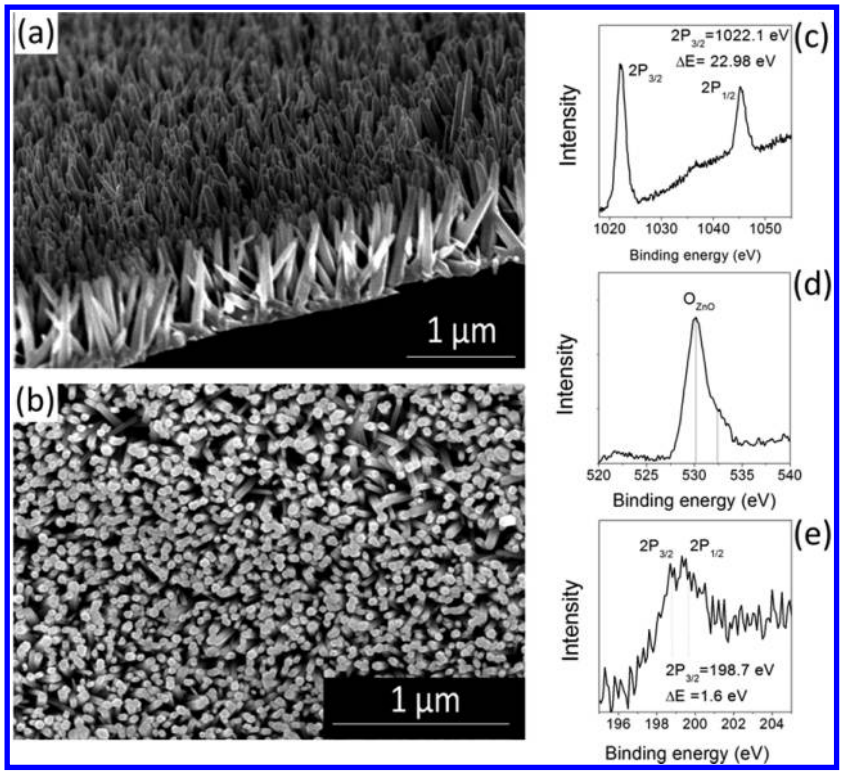

Figure 1. (a) Cross-sectional and (b) top-down SEM images of ZnO:Cl nanowires. (c) Zinc region, (d) oxygen region, and (e) chlorine region of the XPS spectra of ZnO:Cl nanowires.

prepared by vapor-phase transport,[41] pulsed laser deposition,[42] or chemical vapor deposition.[43] However, alternative solution-growth methods, such as chemical bath deposition[44,45] and electrochemical deposition,[46,47] are more suitable for the preparation of large areas of aligned NWs arrays with controlled doping concentrations, at low temperatures, and at high production rates and yields.

In this work, the PL properties of solution-grown ZnO NWs are characterized. In particular, the dependence of the UV and visible PL band intensities on the surface band bending is analyzed and detailed. Evidence of a strong dependence of the yellow and orange emission on the extension of the surface depletion layer is revealed and discussed.

2. EXPERIMENTAL SECTION

NWs Growth. ZnO NWs were electrochemically grown in an aqueous solution inside a three-electrode cell. The growth solution was prepared by incorporating 10 mL of a 0.1 M aqueous solution (Milli-Q+, 18.2 MΩ·cm) of zinc nitrate ($Zn(NO_3)_2{\cdot}4H_2O$) and 10 mL of a 0.1 M aqueous solution of methenamine ($C_6H_{12}N_4$) in 80 mL of deionized water and quickly heating up the solution to 90 °C on a hot plate. A platinum wire immersed in the solution was used as a counter electrode. An Ag/AgCl electrode in saturated KCl (3 M) was used as the reference electrode. A negative dc potential in the range between −0.4 and −1.4 V relative to the reference electrode was applied to a soda-lime glass substrate coated with fluorine-doped tin oxide (FTO), indium-doped tin oxide (ITO), or Pt, which was used as a substrate for the ZnO NWs growth. After 1 h of growth time, the samples were immediately rinsed with deionized water. Chlorine ions were introduced in a controlled manner by replacing part of the deionized water with a 1 M aqueous solution of ammonium chloride (NH_4Cl). To obtain the coaxial ZnO:Cl/ZnO homojunction NWs, the initial ZnO:Cl NWs were thoroughly washed and subsequently subjected to additional electrodeposition growth steps in the absence of NH_4Cl. The applied potential was fixed at −0.4 V vs Ag/AgCl. The thickness of the ZnO shell could be controlled by the electrodeposition time (300 s) and/or the number (1−5) of additional electrodeposition growth steps.

Characterization. Field emission scanning electron microscopy (SEM) was used to characterize the morphology of the obtained materials and measure the density of NWs and their length and width distributions. Both cross-sectional and top-down views were obtained using a FEI Nova Nanosem 230. X-ray photoelectron spectroscopy (XPS) spectra were obtained using a *SPECS SAGE ESCA* system employing Mg Kα (E = 1253.6 eV) with a supplied power of 203 W as the X-ray source. The general spectra were scanned to confirm the presence of Zn, O, and Cl with 30 eV pass energy and 0.5 eV steps. High-resolution scans were obtained to provide information regarding the bonding environment and oxidation states of Zn, O, and Cl. These scans were performed with 15 eV pass energy and 0.10 eV steps. All spectra were shifted to account for sample charging using carbon at 284.80 eV as a reference. Room-temperature PL measurements were obtained using a Kimmon IK Series HeCd CW laser (325 nm and 40 mW). Light was dispersed through an Oriel Corner Stone 1/8 74000 monochromator, detected with a Hamamatsu R928 photomultiplier, and amplified through a Stanford Research Systems SR830 DSP lock-in amplifier. The dependence of the PL intensity on an external applied field was measured by introducing the NWs inside a quartz electrochemical cell. Potential was applied using a three-electrode potentiostat system with an Ag/AgCl electrode in saturated KCl (3 M) as

dx.doi.org/10.1021/jp302443n | J. Phys. Chem. C 2012, 116, 19496−19502

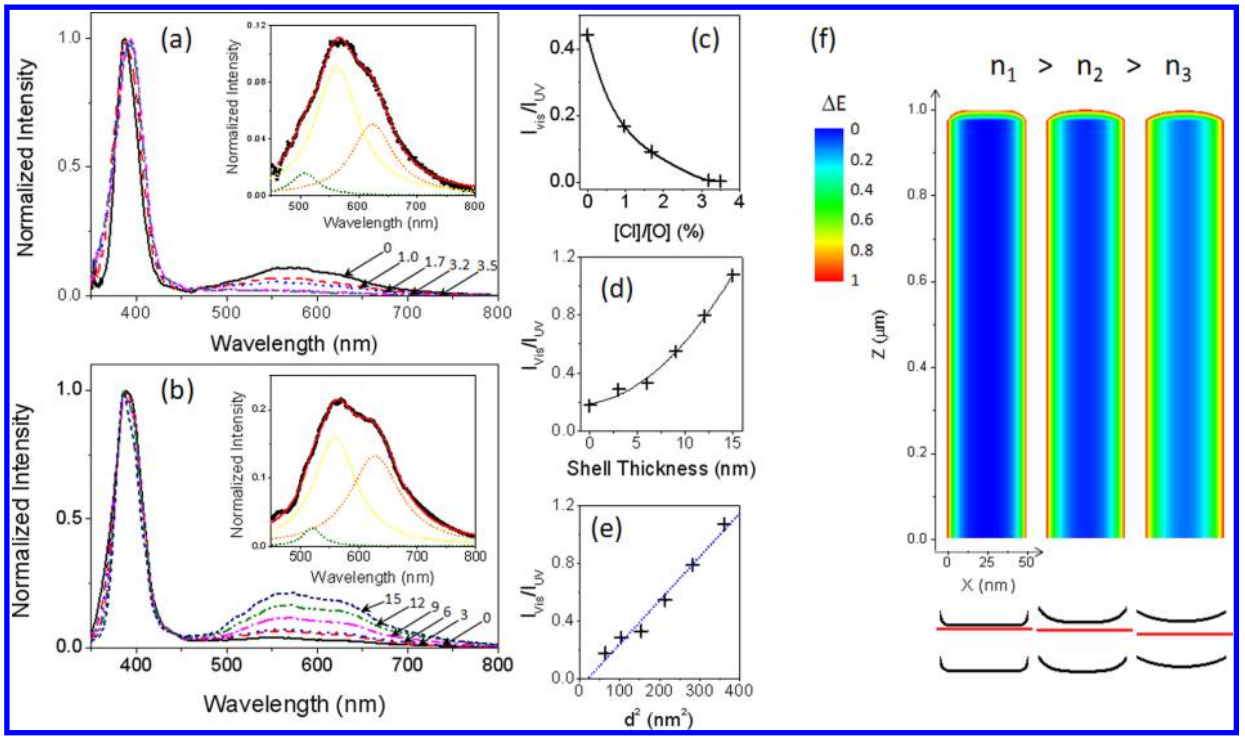

Figure 2. (a) Room-temperature photoluminescence spectra of ZnO:Cl nanowires with different Cl concentrations. The ratios [Cl]/[O], as measured by XPS, were 0, 1.0, 1.7, 3.2 and 3.5%. Inset shows the visible emission in more detail and the fitting of the different emission bands. (b) Room-temperature photoluminescence spectra of ZnO:Cl nanowires and ZnO:Cl/ZnO homojunction nanowires with increasingly thicker shells: 0, 3, 6, 9, 12, and 15 nm. (c) Chlorine dependence of the PL intensity ratio between the UV and visible bands. (d) Shell-thickness dependence of the PL intensity ratio between the UV and visible bands. (e) Dependence of the UV−vis emission intensity ratio on the square of the estimated depletion layer thickness. (f) Schematic view of the energy levels variation across nanowires with different carrier concentrations.

the reference electrode and a Pt wire as counter electrode. A 0.1 M Na_2SO_4 aqueous solution was used as electrolyte.

3. RESULTS AND DISCUSSION

Parts a and b of Figure 1 show representative top-down and cross-sectional SEM images of an array of vertically aligned and single-crystal ZnO:Cl NWs grown by electrodeposition along the ⟨0001⟩ direction. The ZnO:Cl NWs had an average diameter of 170 nm and an average length of 2.3 μm. A controlled concentration of chlorine ions was introduced by dissolving the required amount of ammonium chloride inside the electrodeposition solution. The concentration and chemical state of chlorine ions within the ZnO structure were analyzed by XPS (Figure 1c−e). Chlorine ions are well-known to act as n-type impurities within the ZnO structure. Thus controlling the amount of chlorine, the ZnO:Cl charge carrier concentration could be adjusted in the range from 10^{17} to 10^{20} cm^{-3}.[47]

The room-temperature PL spectra of ZnO:Cl NWs having different doping concentrations are shown in Figure 2a. A strong UV peak, associated with the band-to-band recombination, is clearly seen at 390 nm. The slight red shift of the UV emission peak with the Cl doping concentration may be related to a small band gap narrowing associated with the high density of charge carriers introduced in the ZnO crystal structure or to the preponderance in the PL emission spectra of ZnO:Cl NWs of an exciton slightly below the conduction band edge.[47,48] A broad emission band in the visible part of the spectra is also observed. The visible band has at least two contributions centered at approximately 570 nm (yellow) and 620 nm (orange). A third band, centered at 510 nm (green), could be also fitted (Figure 2a). Similar bands are commonly observed in solution-processed ZnO nanoparticles and nanowires.[18,33] Our experimental results show that when increasing the doping concentration, the relative intensity of the broad visible band decreases with respect to the UV emission band (Figure 2a and c). The doping concentration affected the two main visible contributions, yellow and orange, in a similar way. However, the intensity of the potential green band was not influenced by the doping concentration.

In Figure 2b, the room-temperature PL spectra of ZnO:Cl/ZnO core−shell NWs having different shell thicknesses are plotted. These homojunction ZnO:Cl/ZnO NWs were produced by a two-step electrodeposition process. The [Cl]/[O] ratio of the ZnO:Cl core measured by XPS was 3.2%. The PL spectra obtained from these NW arrays was very similar to those measured from ZnO:Cl NWs. However, in this case, the relative intensity of the visible band increased with the thickness of the intrinsic ZnO shell (Figure 2b and d). This increase was correlated with the thickness of the calculated surface depletion layer (Figure 2e). Again, the shell thickness seems to affect the two main visible contributions, yellow and orange, in the same direction.

Both experimental observations can be explained using the same model. It is well-known that the electrical and optical properties of wide band gap oxide semiconductors are highly susceptible to the surrounding gas atmosphere. In ambient conditions, the surface of ZnO NWs is covered by ionized oxygen species and hydroxyl groups that trap conduction band electrons. This negative surface charge distribution causes an upward bending of the ZnO energy bands at the surface. The surface barrier height depends on the relative position of the chemisorbed species energy levels with respect to the ZnO

dx.doi.org/10.1021/jp302443n | J. Phys. Chem. C 2012, 116, 19496−19502

Fermi level. On the other hand, the width of the depletion layer is strongly dependent on the doping concentration and can be estimated by solving the Poisson equation

$$d = \left[\frac{2\varepsilon\varepsilon_0\Phi_s}{e^2 N_D}\right]^{1/2} \quad (1)$$

where ε is the ZnO relative dielectric constant (8.7), ε_0 is the vacuum permittivity, Φ_s is the height of potential barrier, e is the electron charge, and N_D is the donor concentration. For ZnO in ambient atmosphere, the barrier height is typically close to 0.55 eV.[17] While highly conducting ZnO:Cl NWs are able to screen the surface charge within a very thin surface depletion layer, undoped ZnO NWs are characterized by much thicker depletion regions. In this regard, the width of the depletion layer is calculated to be 70 nm for ZnO with a donor concentration of 10^{17} cm^{-3} and less than 2 nm for a carrier concentration of 10^{20} cm^{-3}.[10,49−52]

As illustrated in Figure 2c, the variation of the relative visible PL band intensity with the doping concentration correlates well with the reduction of the estimated thickness of the surface depletion layer required to screen the surface charge. At the same time, in core−shell nanowires, the presence of an undoped ZnO shell on the surface of highly doped ZnO:Cl NWs allowed increasing the thickness of the depletion layer while conserving a highly conductive core. The visible PL band increased with the thickness of the surface depletion layer (Figure 2d and e). These two evidences were indirect demonstrations that the yellow and orange PL bands obtained from solution-grown ZnO NWs had their origin at the NW surface.

To obtain direct evidence of the influence of the surface depletion layer on the relative intensity of the visible band and discard the influence of other chemical, structural, or geometrical parameters, the PL properties of ZnO:Cl NWs were characterized while adjusting their surface band bending by means of an applied potential.[53−55] For this purpose, the ZnO:Cl NWs were immersed inside a quartz electrochemical cell filled with a 0.1 M Na_2SO_4 aqueous solution as electrolyte. A potential was applied using a three-electrode potentiostat system with an Ag/AgCl electrode in saturated KCl (3 M) as the reference electrode and a Pt wire as counter electrode (Figure 3). When immersing a semiconductor electrode in a redox electrolyte, a gradient of electrochemical potential across the interface exists. The polarization of the ZnO:Cl NWs immersed in the electrolyte shifts the energy bands upward/downward in the NW core, altering in this way the surface band bending, as illustrated in Figure 4b and c. In these conditions, a controllable gradient of electrochemical potential across the interface can be created.

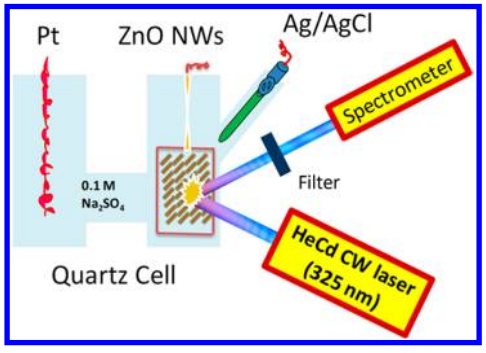

Figure 3. Schematic illustration of the setup used to measure the photoluminescence spectra of ZnO:Cl nanowires under polarization. ZnO:Cl nanowires were immersed in a 0.1 M Na_2SO_4 aqueous solution inside a quartz electrochemical cell. A potential was applied to the ZnO:Cl nanowire-based photoelectrodes using a three-electrode potentiostat system with an Ag/AgCl electrode in saturated KCl (3 M) as the reference electrode and a Pt wire as counter electrode.

Positive potentials shift the energy levels of the NW core downward, thus increasing the potential barrier between the core and the pinned surface states. In these conditions, the anodic current associated with the injection of photogenerated holes from the semiconducting electrode to the electrolyte is extremely small in the dark (Figure 4a). This is because of the lack of holes in the n-type ZnO:Cl electrode. If holes are photogenerated within the ZnO:Cl electrode, an anodic photocurrent is measured at all anodic potentials. As illustrated in Figure 4b, positive potentials facilitate the separation of electron−hole pairs by extending the charge depletion layer where a build-in electric field drives holes toward the electrolyte and electrodes toward the substrate through the ZnO:Cl NW core. Thus the measured photocurrent increases with the positive applied potential, until reaching a saturation photocurrent that depends on the illumination intensity.[56]

Negative applied voltages shift up the energy bands at the NW core, reducing in this way the surface band bending. Such a decrease of the surface depletion layer results in a reduction of the measured photocurrents. At sufficiently high negative polarizations, negative currents are measured, corresponding to the injection of electrons from the semiconductor to the electrolyte (Figure 4c).

Figure 5 shows the room-temperature PL spectra at different applied potentials of a ZnO:Cl NW array immersed inside the electrochemical cell. At positive applied potential, the intensity of both UV and visible bands significantly decreased (Figure 5c). There is an obvious competition between the radiative recombination of electron−hole pairs photogenerated upon UV illumination and the extraction of minority carriers (Figure 4b). This competition could explain a reversible quenching of PL when increasing the positive applied voltage. However, the PL quenching with the positive potential was not reversible. A visual examination of the layer after PL characterization at positive applied voltages revealed the decomposition of the ZnO NWs. A detailed SEM exploration of the area exposed to the UV light revealed that ZnO NWs had been mostly dissolved with the relatively high photocurrents generated by the combination of the strong UV laser radiation and the positive applied potential (Supporting Information Figure S1).[57] At the edge of the UV-exposed area, ZnO nanotubes were observed. The conservation of the ZnO NWs in the nonexposed area demonstrated that the UV exposure was necessary to dissolve the ZnO nanowires. The ZnO spectro-electrochemical dissolution could result from a reverse electrosynthesis reaction at positive potentials under UV illumination. Similar photoelectrochemical dissolution reactions have been previously repoted.[55]

On the other hand, when changing the applied potential toward negative values, the intensity of the visible band clearly decreased. At the same time, the UV emission peak intensity evidently increased (Figure 5a, b). The variation of the visible band intensity affected both yellow and orange contributions in a similar way. It is worth noting that the PL spectra evolution with the applied voltage was reversible, allowing the recovery of the initial spectra when reducing the applied negative voltage.

dx.doi.org/10.1021/jp302443n | J. Phys. Chem. C 2012, 116, 19496−19502

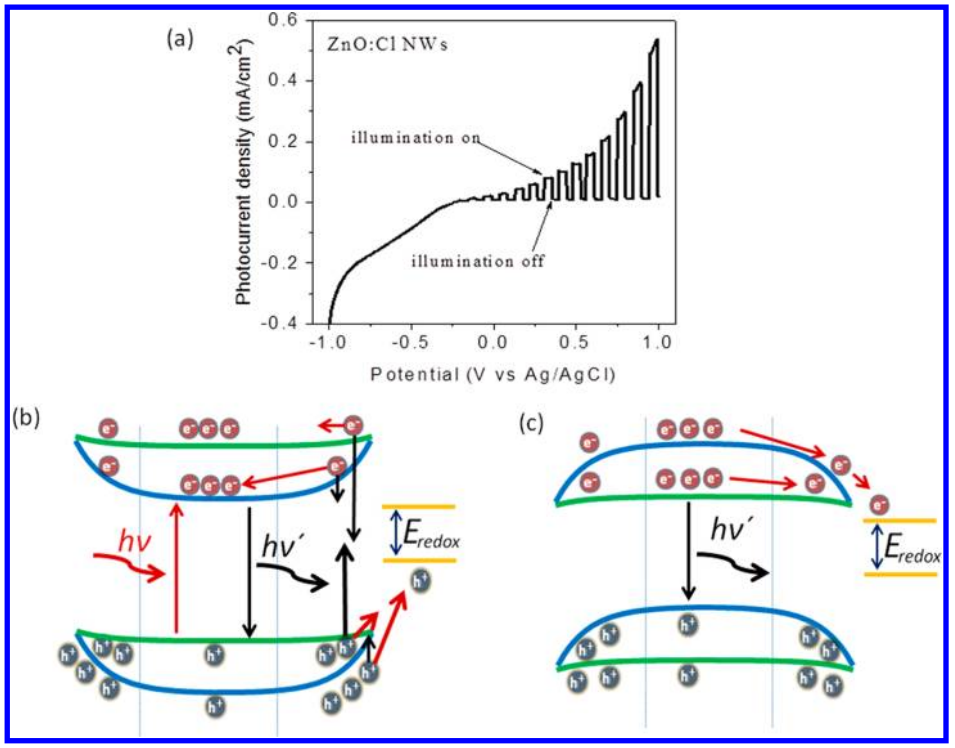

Figure 4. (a) Photocurrent density vs applied potential (V vs Ag/AgCl) for ZnO:Cl NWs measured under chopped UV illumination in a 0.1 M Na_2SO_4 aqueous solution. (b) Representation of the effects of band bending on the competing evolution of electron−hole separation (red arrow) and recombination (black arrow) process at positive applied potential. (c) Representation of the effects of band bending on the electrochemical photoluminescence induced by electron−hole recombination at negative applied potential. Intraband gap states were omitted for simplicity.

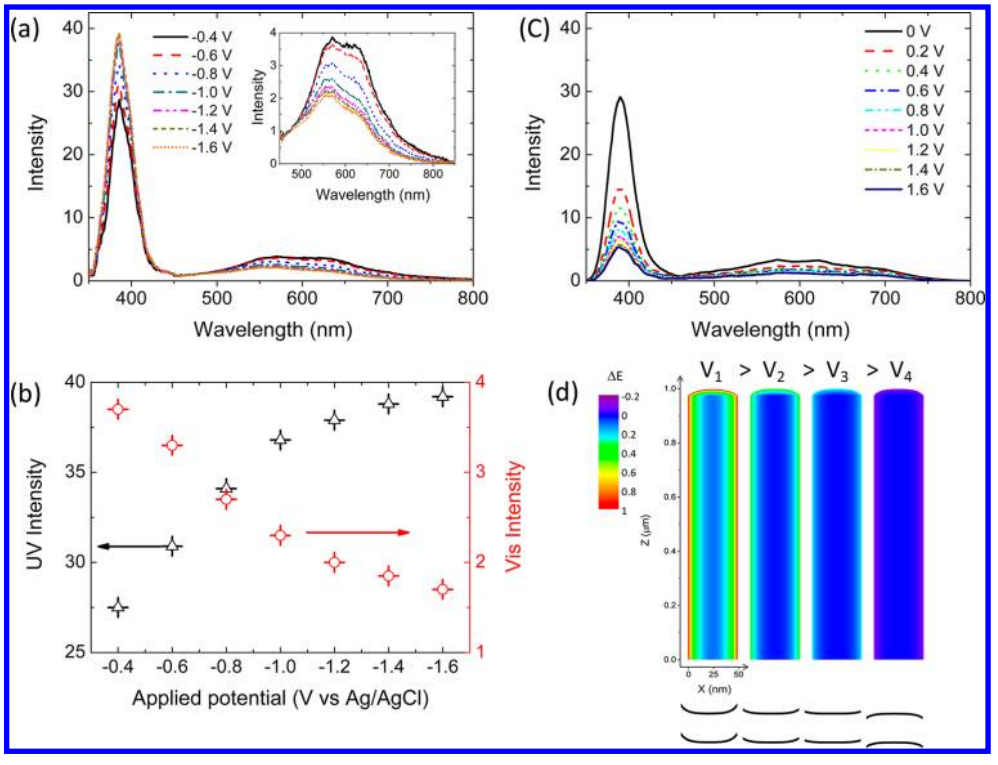

Figure 5. (a) Room-temperature photoluminescence spectra of ZnO:Cl nanowires at different negative potential. Inset shows the visible emission in more detail. (b) Evolution of UV and visible emission intensities with the applied potential. (c) Room-temperature photoluminescence spectra of ZnO:Cl nanowires at positive potentials. (d) Schematic view of the energy level variation across nanowires polarized at different potentials.

These results evidence that orange and yellow PL bands obtained from solution-grown ZnO NWs were strongly dependent on the surface band bending. Yellow and orange emissions were previously associated with transitions from the conduction band, donor OH^- states, or zinc interstitials to oxygen interstitials or zinc vacancies.[18,33,58] The results

dx.doi.org/10.1021/jp302443n | J. Phys. Chem. C 2012, 116, 19496−19502

reported here do not allow determination of the specific chemical identity of the trap state, but evidence their surface localization. The electric field inside the depletion layer helps to separate photogenerated electron−hole pairs, driving electrons to the bulk and holes to the surface. The contribution from states localized directly at the ZnO surface would increase with the extension of the surface depletion layer because of the higher amount of holes harvested. On the other hand, hole accumulation at the depletion layer, localized either in the valence band or in defect states, such as ionized oxide vacancies, could also activate radiative states not active within the nanocrystal bulk. A third possibility is the slowdown of band-to-band transitions at the depletion region due to the existence of a driving force for exciton separation. In this scenario, slower radiative recombination processes with much lower efficiencies in the ZnO bulk would be promoted at the ZnO surface (Figure 6a).

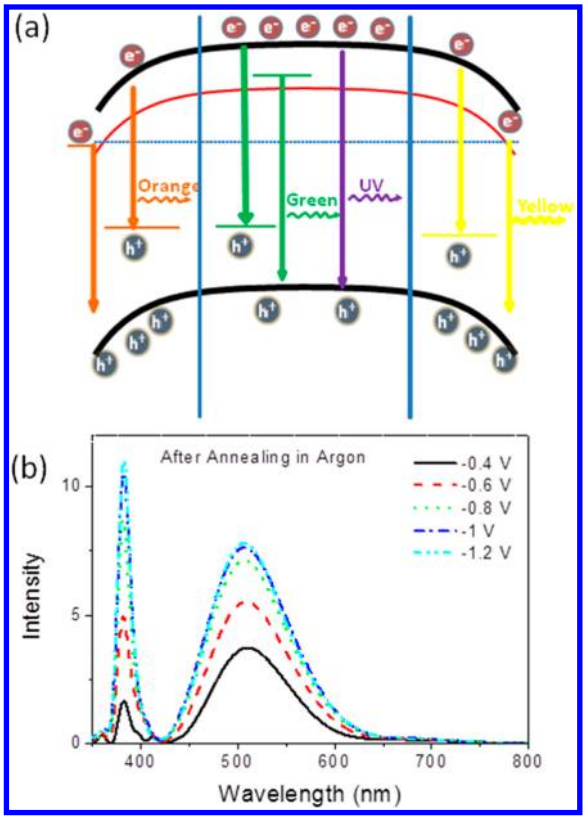

Figure 6. (a) Schematic of the possible localization of the states contributing to the visible emission within ZnO nanowires. (b) Room-temperature photoluminescence spectra of annealed ZnO:Cl nanowires at increasingly higher negative potentials.

Finally, the ZnO NW arrays obtained by electrodeposition were annealed in argon at 450 °C during 1 h. The morphology and composition of ZnO:Cl NWs before and after annealing were analyzed using the exact same sample (Supporting Information Figure S3). The O/Zn atomic ratio was 1.76 before annealing and 1.62 after annealing, as measured by EDX. It should be pointed out that the measured O/Zn atomic ratios were influenced by the ITO-covered glass substrate. However, results obtained from the exact same sample before and after annealing clearly pointed out toward a decrease of the oxygen concentration with the annealing treatment in argon. This decrease could be attributed to the decomposition of $Zn(OH)_2$ to ZnO and/or the desorption of chemisorbed oxygen or hydroxyl groups from the ZnO NWs surface with the annealing process.

The annealing treatment substantially modified the PL spectra. Figure 6b shows the room-temperature PL spectra obtained from the annealed NWs. The UV peak corresponding to band-to-band recombination and a relatively broad visible band could be easily identified. The intensity of both bands clearly increased with the annealing process mainly due to the improvement of the crystalline structure and the removal of nonradiative defects (Supporting Information Figure S2). At the same time, the relative intensity of the visible band increased considerably. However, in this case, the visible band showed only one contribution, centered at around 510 nm (green). Such emission at 510 nm has been previously associated with transitions involving oxygen vacancies and zinc interstitials.[59]

It is generally accepted that annealing in argon facilitates the removal of chemisorbed oxygen or other oxygen-containing species (e.g., OH^-) from the ZnO surface, reducing the defect concentration and the charge depletion region and thus enhancing the UV emission.[60] The decrease of the yellow and orange emission intensities with the annealing process is also consistent with the reduction of the defect concentration. In particular, the defects at the origin of these emissions are clearly eliminated with the annealing treatment. On the other hand, the relatively strong green emission obtained after the annealing process can be associated with the decrease of the oxygen concentration and the consequent increase of the concentration of oxygen vacancies and zinc interstitial defects with the annealing process in an inert atmosphere.

The PL spectra measured under electrical polarization showed that both the UV and green bands increased with the negative potential (Figure 6b). This general feature is in good agreement with an earlier report on electroluminescence spectroscopy of polycrystalline ZnO electrode and can be explained by the injection of minority carriers from the electrolyte to the semiconductor.[61] These results point toward the bulk localization of the states at the origin of the green PL emission in annealed ZnO NWs obtained by solution-processing methods. As in the case of as-grown ZnO NWs, the annealed arrays were not stable at positive potential when exposed to UV light.

4. CONCLUSIONS

Three sets of measurements were performed to demonstrate the strong dependence of the visible PL emission in solution-grown ZnO NWs on the thickness of the surface depletion region. The results obtained indicate that the orange and yellow emission bands originate from transitions taking place between states localized at or near the NW surface. On the other hand, the green emission measured from annealed ZnO NWs showed no dependence on the extension of the surface depletion layer and followed the same trend as the UV emission, which points toward its origin in the bulk.

■ ASSOCIATED CONTENT

Ⓢ Supporting Information

PL spectrum of ZnO:Cl NWs before and after annealing at 0 V, SEM images, and EDX results. This material is available free of charge via the Internet at http://pubs.acs.org.

dx.doi.org/10.1021/jp302443n | J. Phys. Chem. C 2012, 116, 19496−19502

AUTHOR INFORMATION

Corresponding Author

*E-mail address acabot@irec.cat; tel. +34625615115.

Notes

The authors declare no competing financial interest.

ACKNOWLEDGMENTS

The research was supported by the European Regional Development Funds and by the Spanish MICINN projects MAT2008-05779, MAT2008-03400-E/MAT, MAT2010-15138, MAT2010-21510, CSD2009-00050, and ENE2008-03277-E/CON. J.F. is thankful for the FI-DGR grant from the Agència de Gestió d'Ajuts Universitaris i de Recerca (AGAUR) from the Catalan Government. A.C. is thankful for financial support through the Ramón y Cajal program to the Spanish MICINN.

REFERENCES

(1) Tsukazaki, A.; Ohtomo, A.; Onuma, T.; et al. *Nat. Mater.* **2005**, *4*, 42−46.
(2) Pauproté, T.; Lincot, D.; Viana, B.; Pellé, F. *Appl. Phys. Lett.* **2006**, *89*, 233112.
(3) Claude, L. C.; Ramon, T. Z.; Ryan, M. A. *Adv. Mater.* **2005**, *17*, 1512−1515.
(4) Djurišić, A. B.; Leung, Y. H. *Small* **2006**, *2*, 944−961.
(5) Güell, F.; Ossó, J. O.; Goñi, A. R.; Cornet, A.; Morante, J. R. *Superlattice. Microstruct.* **2009**, *45*, 271−276.
(6) Güell, F.; Ossó, J. O.; Goñi, A. R.; Cornet, A.; Morante, J. R. *Nanotechnology* **2009**, *20*, 315701.
(7) Zheng, M. J.; Zhang, L. D.; Li, G. H.; Shen, W. Z. *Chem. Phys. Lett.* **2002**, *363*, 123−128.
(8) Vanheusden, K.; Seagera, C. H.; Warren, W. L.; Tallant, D. R.; Caruso, J.; Hampden-Smithb, M. J.; Kodasb, T. T. *J. Lumin.* **1997**, *75*, 11−16.
(9) Vanheusden, K.; Warren, W. L.; Seager, C. H.; Tallant, D. R.; Voigt, J. A.; Gnade, B. E. *J. Appl. Phys.* **1996**, *79*, 7983−7990.
(10) Liao, Z. -M.; Zhang, H.-Z.; Zhou, Y.-B.; Xu, J.; Zhang, J.-M.; Yu, D.-P. *Phys. Lett. A* **2008**, *372*, 4505−4509.
(11) Bouzid, K.; Djelloul, A.; Bouzid, N.; Bougdira, J. *Phys. Status Solidi A* **2009**, *206*, 106−115.
(12) Vanheusden, K.; Seager, C. H.; Warren, W. L.; Tallant, D. R.; voigt, J. A. *Appl. Phys. Lett.* **1996**, *68*, 403−405.
(13) Ahn, M.-W.; Park, K.-S.; Heo, J.-H.; Park, J.-G.; Kim, D.-W.; Choi, K. J.; Lee, J.-H.; Hong, S.-H. *Appl. Phys. Lett.* **2008**, *93*, 263103.
(14) Van Dijiken, A.; Meulenkamp, E. A.; Vanmaekelberg, D.; Meijerink, A. *J. Phys. Chem. B* **2000**, *104*, 4355−4360.
(15) Fan, X. M.; Lian, J. S.; Jiang, Q.; Zhou, Z. W. *J. Mater. Sci.* **2007**, *42*, 2678−2683.
(16) Chang, S.-S. *J. Korean Ceram. Soc.* **2011**, *48*, 251−256.
(17) Lin, B.; Fu, Z.; Jia, Y. *Appl. Phys. Lett.* **2001**, *79*, 943−945.
(18) Manzano, C. V.; Alegre, D.; Caballero-Calero, O.; Alén, B.; Martín-González, M. S. *J. Appl. Phys.* **2011**, *110*, 043538.
(19) Janotti, A.; Van de Walle, C. G. *Phys. Rev. B* **2007**, *76*, 165202.
(20) Roro, K. T.; Dangbegnon, J. K.; Sivaraya, S.; Leitch, A. W. R.; Botha, J. R. *J. Appl. Phys.* **2008**, *103*, 053516.
(21) Liua, Z. W.; Ong, C. K.; Yu, T.; Shen, Z. X. *Appl. Phys. Lett.* **2006**, *88*, 053110.
(22) Zeng, H.; Duan, G.; Li, Y.; Yang, S.; Xu, X.; Cai, W. *Adv. Funct. Mater.* **2010**, *20*, 561−572.
(23) Garces, N. Y.; Wang, L.; Bai, L.; Giles, N. C.; Halliburton, L. E.; Cantwell, G. *Appl. Phys. Lett.* **2002**, *81*, 622−624.
(24) Gu, X.; Huo, K.; Qian, G.; Fu, J.; Chu, P. K. *Appl. Phys. Lett.* **2008**, *93*, 203117.
(25) Andelman, T.; Gong, Y.; Polking, M.; Yin, M.; Kuskovsky, I.; Neumark, G.; O'Brien, S. *J. Phys. Chem. B* **2005**, *109*, 41314−14318.
(26) Shalish, I.; Temkin, H.; Narayanamurti, V. *Phys. Rev. B* **2004**, *69*, 245401.
(27) Chang, P.-C.; Chien, C.-J.; Stichtenoth, D.; Ronning, C.; Lu, J. G. *Appl. Phys. Lett.* **2007**, *90*, 113101.
(28) Van Dijken, A.; Meulenkamp, E. A.; Vanmaekelbergh, D.; Meijerink, A. *J. Phys. Chem. B* **2000**, *104*, 1715−1723.
(29) Yousefi, R.; Kamaluddin, B. *J. Alloys Compd.* **2009**, *479*, 11−14.
(30) Wu, X. L.; Siu, G. G.; Fu, C. L.; Ong, H. C. *Appl. Phys. Lett.* **2001**, *78*, 2285−2287.
(31) Djurišić, A. B.; Leung, Y, H.; Choy, W. C. H.; Cheah, K. W.; Chan, W. K. *Appl. Phys. Lett.* **2004**, *84*, 2635−2637.
(32) Richters, J.-P.; Voss, T.; Kim, D. S.; Scholz, R.; Zacharias, M. *Nanotechnology* **2008**, *19*, 305202.
(33) Shi, S.; Xu, J.; Zhang, X.; Li, L. *J. Appl. Phys.* **2011**, *109*, 103508.
(34) Ye, J. D.; Gu, S. L.; Qin, F.; et al. *Appl. Phys. A: Mater. Sci. Process.* **2005**, *81*, 759−762.
(35) Fan, J.; Guell, F.; Fabrega, C.; Shavel, A.; Carrete, A.; Andreu, T.; Morante, J. R.; Cabot, A. *Appl. Phys. Lett.* **2011**, *99*, 262102.
(36) House, R. L.; Mehl, B. P.; Kirschbrown, J. R.; barnes, S. C.; Papanikolas, J. M. *J. Phys. Chem. C* **2011**, *115*, 10806−10816.
(37) Yang, L. L.; Zhao, Q. X.; Israr, M. Q.; Sadaf, J. R.; Willander, M.; Pozina, G.; Yang, J. H. *J. Appl. Phys.* **2010**, *108*, 103513.
(38) Ahn, C. H.; Kim, Y. Y.; Kim, D. C.; Mohanta, S. K.; Cho, H. K. *J. Appl. Phys.* **2009**, *105*, 013502.
(39) Wang, Z. L. *J. Phys.: Condens. Matter.* **2004**, *16*, 829−858.
(40) Chu, D.; Masuda, Y.; Ohji, T.; Kato, K. *J. Am. Ceram. Soc.* **2010**, *93*, 887−893.
(41) Huang, M. H.; Wu, Y.; Feick, H.; Tran, N.; Weber, E.; Yang, P. *Adv. Mater.* **2001**, *13*, 113−116.
(42) Sun, Y.; Fuge, G. M.; Ashfold, M. N. R. *Chem. Phys. Lett.* **2004**, *396*, 21−26.
(43) Park, W. I.; Kim, D. H.; Jung, S. W.; Yi, G. C. *Appl. Phys. Lett.* **2002**, *80*, 4232−4234.
(44) Grene, L. E.; Yuhas, B. D.; Law, M.; Zitoun, D.; Yang, P. *Inorg. Chem.* **2006**, *45*, 7535−7543.
(45) Govender, K.; Boyle, D. S.; Kenway, P. B.; ÓBrien, P. *J. Mater. Chem.* **2004**, *14*, 2575−2591.
(46) Peulon, S.; Lincot, D. *Adv. Mater.* **1996**, *8*, 166−170.
(47) Fan, J.; Shavel, A.; Zamani, R.; Fábrega, C.; et al. *Acta Mater.* **2011**, *59*, 6790−6800.
(48) Egelhaaf, H.-J; Oelkrug, D. *J. Cryst. Growth* **1996**, *161*, 190−194.
(49) Liao, Z.-M.; Liu, K.-J.; Zhang, J.-M.; Xu, J.; Yu, D.-P. *Phys. Lett. A* **2007**, *367*, 207−210.
(50) Liao, Z.-M.; Hou, C.; Zhou, Y.-B.; Xu, J.; Zhang, J.-M.; Yu, D.-P. *J. Chem. Phys.* **2009**, *130*, 084708.
(51) Prades, J. D.; Hernandez-Ramirez, F.; Jimenez-Diaz, R.; Manzanares, M.; Andreu, T.; Cirera, A.; Romano-Rodriguez, A.; Morante, J. R. *Nanotechnology* **2008**, *19*, 465501.
(52) Mora-Seró, I.; Fabregat-Santiago, F.; Denier, B.; Bisquert, J.; Tena-Zaera, R.; Elias, J.; Lévy-Clément, C. *Appl. Phys. Lett.* **2006**, *89*, 203117.
(53) Bradley, R. K.; Arthur, B. E. *J. Am. Chem. Soc.* **1980**, *30*, 968−980.
(54) Petermann, G.; Tributsch, H.; Bogomolni, R. *J. Chem. Phys.* **1972**, *57*, 1026−1032.
(55) Noguchi, H.; Kondo, T.; Uosaki, K. *J. Phys. Chem. B* **1997**, *101*, 4978−4981.
(56) Williams, R. *J. Chem. Phys.* **1960**, *32*, 1505−1514.
(57) Gerischer, H. *J. Electrochem. Soc.* **1966**, *113*, 1174−1182.
(58) Djurišić, A. B.; Ng, A. M. C.; Chen, X. Y. *Prog. Quant. Electron.* **2010**, *34*, 191−259.
(59) Liu, X.; Wu, X. H.; Cao, H.; Chang, R. P. H. *J. Appl. Phys.* **2004**, *95*, 3141−3147.
(60) Sun, Y.; George Ndifor-Angwafor, N.; Jason Riley, D.; Ashfold Michael, N. R. *Chem. Phys. Lett.* **2006**, *431*, 352−357.
(61) Fichou, D.; Kossanyi, J. *J. Electrochem. Soc.* **1986**, *133*, 1607−1617.